RSC Advances

ROYAL SOCIETY OF CHEMISTRY

www.rsc.org/advances

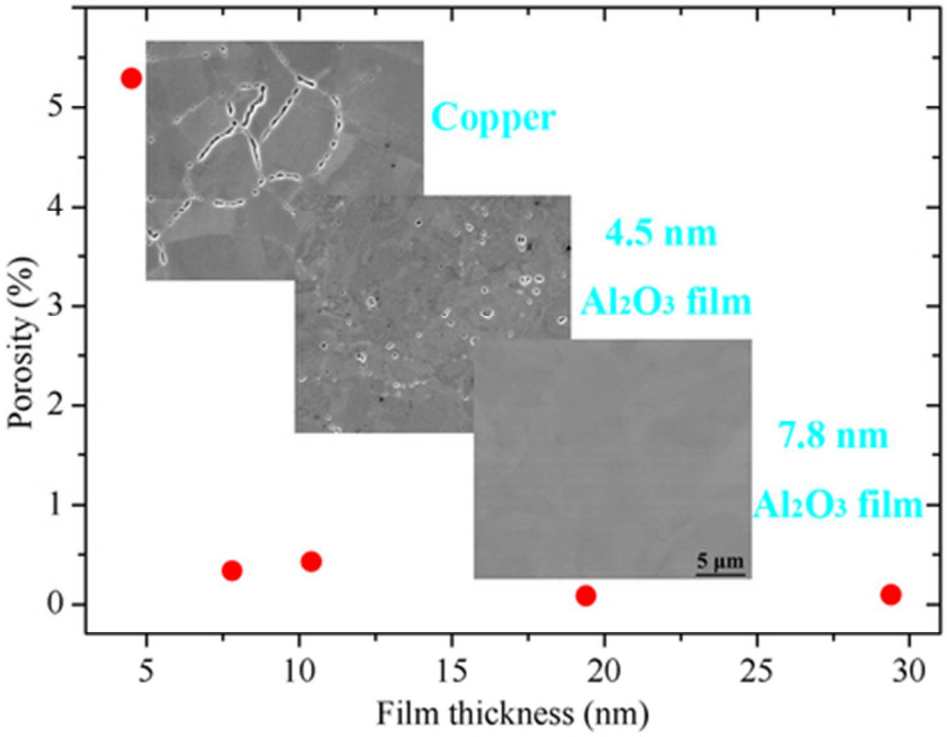

39x31mm (300 x 300 DPI)

Cite this: DOI: 10.1039/c0xx00000x

www.rsc.org/xxxxxx

ARTICLE TYPE

Ultra-thin Al_2O_3 films grown by atomic layer deposition for corrosion protection of copper

Zhimin Chai,[a] Yuhong Liu,[a] Jing Li,[ab] Xinchun Lu*[a] and Dannong He[c]

Received (in XXX, XXX) Xth XXXXXXXXX 20XX, Accepted Xth XXXXXXXXX 20XX

DOI: 10.1039/b000000x

Ultra-thin Al_2O_3 films with thickness in the range of 4.5-29.4 nm were prepared on a copper substrate by atomic layer deposition (ALD) at the temperature of 150 °C to protect the substrate from corrosion. Auger electron spectrum (AES) was employed to analyze elemental components of the film surface and to detect elemental distribution in a depth direction of the film, and atomic force microscope (AFM) and scanning electron microscopy (SEM) were employed to measure the surface morphology before and after corrosion experiment. Electrochemical impedance spectroscopy (EIS) was used to measure anti-corrosion property of the film in a 0.1 M NaCl solution. The results demonstrate that high quality ultra-thin Al_2O_3 films with a uniform in-depth stoichiometry are achieved on the copper substrate and the films can efficiently decrease the corrosion of copper. A thicker Al_2O_3 film can provide better corrosion resistance because of its lower porosity. When the film thickness is 7.8 nm or above, the copper surface can be well protected, which is embodied by the fact that the AFM and SEM images of the surface do not show great difference before and after corrosion.

Keywords: atomic Layer Deposition; Al_2O_3; ultra-thin; anti-corrosion

1. Introduction

Copper, a technically important material with excellent heat conductivity and corrosion resistance,[1] is widely used in plenty of practical applications like heat exchangers[2, 3] and household plumbing system.[4, 5] Although being resistant to corrosion in pure water, it is subject to corrosion in aggressive media, such as Cl^- and SO_4^{2-}.[6-8] One efficient way to decrease the corrosion is to grow a protective coating to separate copper from the corrosive media. Al_2O_3 film, possessing excellent insulation properties, is a good choice for the protective coating.[9]

Atomic layer deposition (ALD), a process derived from chemical vapor deposition (CVD), is a proper candidate used to grow a compact Al_2O_3 film which is nearly pinhole free.[10, 11] In the ALD process, two precursors are introduced into a reaction chamber alternately and separated by a purge cycle of an inert gas to avoid direct reaction between the precursors. By adjusting ALD parameters, the reaction reaches saturation, making the film growth self-limiting. This self-limiting feature further makes it possible to grow a highly uniform and conformal Al_2O_3 film on a large area, with film thickness controlled at a monolayer level. In addition, both flat and complicated 3D surfaces can be conformally coated with the film.

Because of the low deposition rate of ALD, it takes much time to grow a thick film. Thus, ALD is generally used to grow a thin film with a low thickness of several nanometers.[10] Fortunately, such thin film can still have an excellent sealing property. Ultra-thin Al_2O_3 films with a thickness in a range from 5 to 50 nm were grown by thermal ALD on a stainless steel (316L) substrate,[12] and results of electrochemical measurements (linear scan voltammetry (LSV) and electrochemical impedance spectroscopy (EIS)) revealed that a 50 nm Al_2O_3 film grown at 250 °C achieved the lowest porosity value of 0.03%, and reduced the corrosion current density by four orders of magnitude with respect to the substrate. Due to high residual contamination from the precursors at a low substrate temperature of 160 °C, a 50 nm Al_2O_3 film grown on a carbon steel alloy (AISI 52100) substrate reduced the current density only by two orders of magnitude.[13, 14] Al_2O_3 film was also grown by plasma-enhanced ALD on 100Cr6 mild steel and aluminium Al2024-T3 alloys to provide corrosion protection. As radicals in plasma improve the surface reactivity, the film prepared by plasma-enhanced ALD is denser than that by thermal ALD and thus is better in anti-corrosion property.[15, 16] In spite of the earlier work,[17] to our knowledge, using Al_2O_3 film as the protective coating for copper are rarely practiced.

In the present study, Al_2O_3 films with thickness in the range of of 4.5 to 29.4 nm were prepared by atomic layer deposition (ALD) on a copper and the corrosion resistance property of the coated copper was investigated by electrochemical impedance spectroscopy (EIS) measurement. The composition of the Al_2O_3 films was measured by an Auger electron spectroscopy (AES), and the surface morphology before and after corrosion was observed by a scanning electron microscopy (SEM) and an atomic force microscope (AFM).

2. Experimental

2.1 Ultra-thin film preparation

High purity copper (99.99 wt% purity) with a size of 20×20×2 mm^3 was employed as the substrate to grow ultra-thin Al_2O_3 films. Since surface defect and contamination would give rise to the failure of films,[14, 18] the copper substrate was fine polished to decrease the surface defects. The copper substrate was mechanically polished with SiC foils (Grit size #320, #500 and #1200) followed by a final polishing with commercial slurries (PL-7105, Fujimi) (the slurries were diluted by deionized water with a dilution ratio of 1:3). After polishing, colloidal silica particle contamination on the polished surface was removed by a dilute sulphuric acid solution, and then the copper substrate was cleaned in an ultrasonic bath of deionized water for 2 min and dried by blowing with high pure nitrogen (99.99%). The RMS roughness of the final surface measured by AFM (Veeco) was <1 nm.[19]

The Al_2O_3 film was prepared with a Picosun SUNALE R-150 ALD reactor. Trimethyl aluminum (TMA, purity >99.99%) and water were used as Al precursor and oxidant, respectively. These two precursors were alternately fed into the growth chamber using high purity nitrogen (purity >99.999%) as carrier gas, and between the two precursor pulses, the growth chamber was purged with the high purity nitrogen. One complete ALD cycle consisted of 0.1 s of TMA/N_2, 3 s of N_2, 0.1 s of H_2O/N_2, and 4 s of N_2. During deposition, the temperature in the chamber was 150 °C, and the pressure in the chamber was ~1400 Pa.

2.2 Film characterization

The thickness of Al_2O_3 films was measured from a silicon wafer coated simultaneously with the copper substrate. The measurement was carried out with null-ellipsometry (Multiskop, Optrel). Data fit for thickness and refractive index of the film was carried out using Elli software (Optrel). A 2-layer model comprising silicon and air was used to determine the refractive index and the absorption coefficient of the silicon substrate, and then the film thickness was determined using a 3-layer model comprising silicon, Al_2O_3 film and air. In this study, 30-300 ALD cycles were preformed, and the resulting film thickness is in the range of 4.5 to 29.4 nm.[19]

Auger electron spectrum is a powerful tool to detect the composition of materials. The surface elemental analysis and the elemental depth profile were obtained using AES (PHI-700, ULVAC-PHI) with a co-axial cylindrical mirror analyzer (CMA). The spectrometer was operated at a pressure of $<3.9\times10^{-9}$ Torr. For surface analysis, a 5 kV electron beam with a diameter of 25 nm was employed. The depth profiling was done with a 3 kV Ar ion sputter beam at an incident angle of 30°. The sputtering rate of SiO_2 film (calibration specimen) was 4 nm/min.

2.3 Electrochemical measurements

Corrosion test was conducted using an M237A potentiostat (EG&G) with a conventional three-electrode cell. A platinum wire and a silver/silver chloride (Ag/AgCl) electrode were used as counter and reference electrodes, respectively. A working electrode was placed in a Teflon sample holder and the exposed area was delimited to 2.01 cm^2 by a Viton O-ring. All the experiments were performed in a 0.1 M NaCl solution prepared by ultra-pure water (resistivity >18 MΩcm) and reagent grade chemicals (NaCl Analar Normapur analytical reagent, Sinopharm Chemical Reagent Co.). Before EIS measurement, the sample was immersed in the solution for 30 min to get a stable open circuit potential (OCP), and then the EIS was measured at OCP, in a frequency ranging 10 MHz-100 kHz, with a signal amplitude of 10 mV. Finally, the acquired spectra were analyzed using ZView software.

The surface morphology of samples before and after electrochemical measurement was observed using AFM and SEM (FEI Quanta 200 FEG).

3. Results and discussion

3.1 Film characterization

Figure 1 (a) shows an AFM image of the copper substrate. After polishing, the copper substrate becomes very smooth, its root-mean-square (RMS) roughness reaching 0.72 nm. The copper substrate we used is polycrystalline, and the grain boundary can be clearly seen. Figure 1 (b) shows an AFM image of the copper substrate coated with a 19.4 nm Al_2O_3 film. The two images demonstrate that the morphology of the coated copper substrate does not differ greatly with that of the uncoated copper substrate. This is attributed to the self-limiting growth mechanism of the ALD process which enables conformal coating of the substrate.

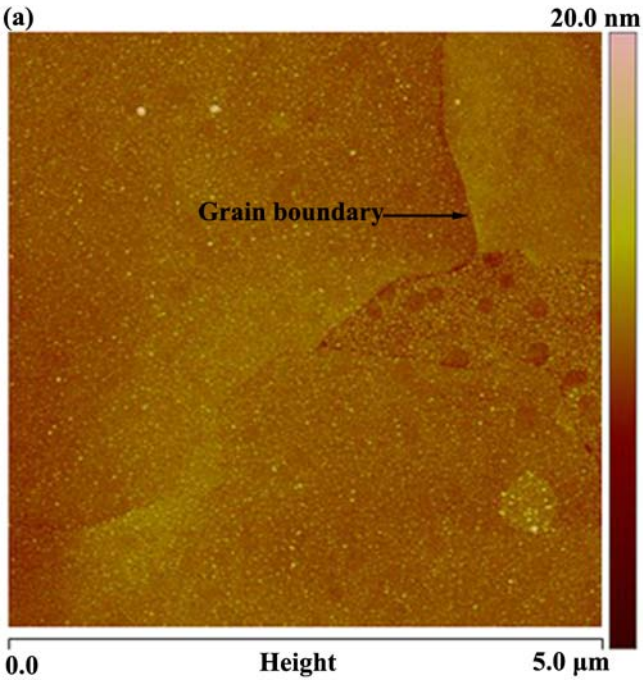

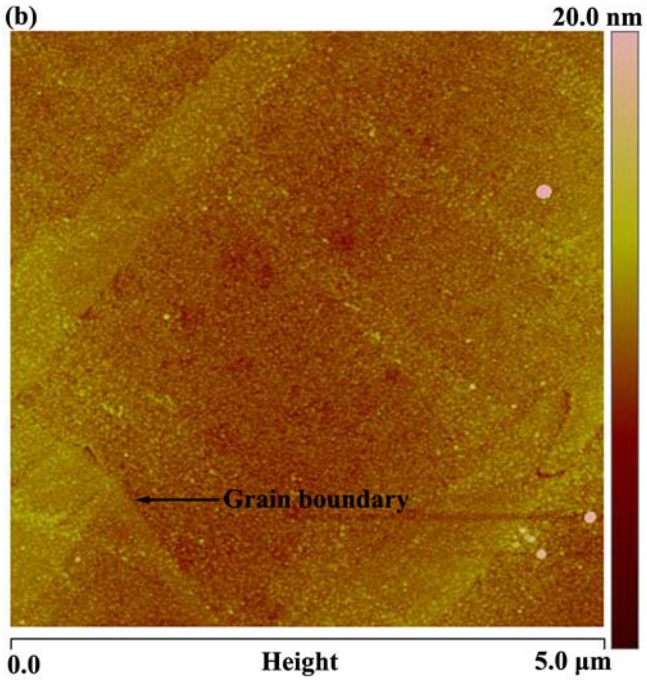

Figure 1. (a) AFM image of the polished copper substrate. (b) AFM image of the polished copper substrate coated with a 19.4 nm Al_2O_3 film.

Figure 2 shows the Auger spectrum of the surface of 19.4 nm Al_2O_3 film coated copper. It can be seen that Al, O and C are present on the surface of the film. For Al, there are two transitions, which are located at 59.0 eV and 1391.0 eV, respectively. Surface atomic concentrations of Al, O and C can be calculated from peak intensities and the atomic concentrations obtained thereof are 28.5, 49.4 and 22.1%, respectively. O/Al atomic ratio calculated from atomic concentration is 1.7 which is larger than 1.5 of stoichiometric Al_2O_3. The large concentration of O is attributed to contamination of surface exposed to the ambient air.

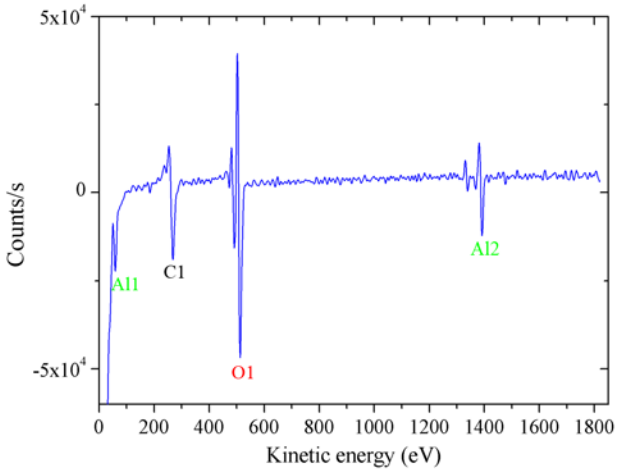

Figure 2. Auger spectrum of the surface of Al_2O_3 film deposited on the copper substrate.

Figure 3 shows the depth profile of the 19.4 nm Al_2O_3 film deposited on the copper substrate. For the Al_2O_3 film, plateaus of O and Al atom concentration are observed, indicating the growth of a film with uniform in-depth stoichiometry. Because of unavoidable exposure to the ambient air before measurement, high concentration of C is present on the very surface of the film. However, after 1 min of sputtering, the concentration decreases to the residual level. The residual C in the film is due to incomplete reaction of $Al(CH_3)_3$ precursor.[20, 12, 21]

After about 6 min of sputtering, the concentrations of Al and O decreases, while the concentration of Cu atom starts to increase, marking the onset of the interface layer. An increase of C atomic concentration is observed in this layer. This is due to organic contamination on the surface of substrate before deposition. The width of the interfacial layer is ~7.5 nm which is much smaller than ~50 nm of previous report.[14] Thin interfacial layer is attributed to the fact that copper substrate was fine polished. Finally, after approximately 8.5 min of sputtering, the concentration of the Cu atom becomes stable indicating the entry of the substrate.

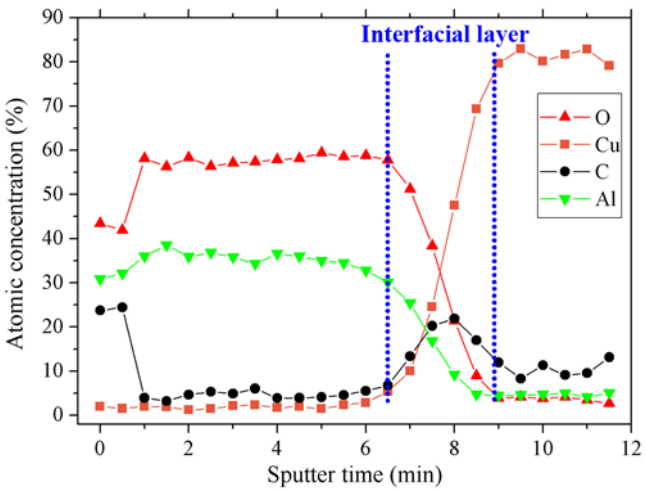

Figure 3. Depth profile of the 19.4 nm Al_2O_3 film deposited on the copper substrate.

3.2 Electrochemical impedance spectroscopy

EIS measurement was employed to investigate the corrosion property of the copper coated with Al_2O_3 film. Figure 4 (a) shows the sketch of the test system. The copper coated with Al_2O_3 film is immersed in a 0.1 M NaCl aqueous solution, and a disturbance sinusoidal voltage $E\sin(\omega t)$ is applied to the system. This system is usually modeled with an equivalent circuit (EC) with two time constants,[22-24] as shown in Figure 4 (b). The parallel-connected elements R_{pore} and CPE_{coat} are pore resistance and coating capacitance which correspond to the dielectric properties of the film. Another pair of parallel-connected elements R_{ct} and CPE_{dl} is charge transfer resistance and double layer capacitance which are adopted to describe the substrate/electrolyte interface in the permeable coating pinholes. R_e is the electrolyte resistance. In this model, a constant phase element (CPE) was used to replace the ideal capacitor. The CPE impedance is defined by Eq. (1),

$$Z_{CPE} = \frac{1}{Q(j\omega)^n} \qquad (1)$$

where Q and n are adjustable parameters obtained from the non-linear fitting. The value of n always lies between 0.5 and 1. Surface roughness was demonstrated to be responsible for the

variation.[24] When a surface is rough, the true area exposed to the solution is larger than that obtained from geometrical calculation, and in this condition, n is not a unity value. While for a perfect capacitance made from two smooth surfaces, the value of n equals 1. Using the Q and n parameters, equivalent capacitance value can be calculated from the Brug equation[25]

$$C = Q^{1/n} R_e^{(1-n)/n} \qquad (2)$$

When the copper substrate is exposed to the ambient air or in the electrolyte, an oxide layer grows on its surface.[26-28] Therefore, the EC for the copper substrate should also consist of two time constants, as shown in Figure 4 (c). In this model, CPE_{coat} and R_{pore} are the dielectric properties of the surface oxide layer. The corrosion of the copper substrate occurs in pinholes in the oxide layer. Because the corrosion of the copper substrate is fast, the reaction byproduct may block the pinholes, which reduces diffusions of reagents (O_2 and Cl^-) and reaction products ($CuCl^{x-}$) towards and away from the active zones.[29-33] In this situation, the corrosion is controlled not only by a charge transfer process but also by a mass diffusion process. The diffusion process is modeled by a diffusion impedance (W).

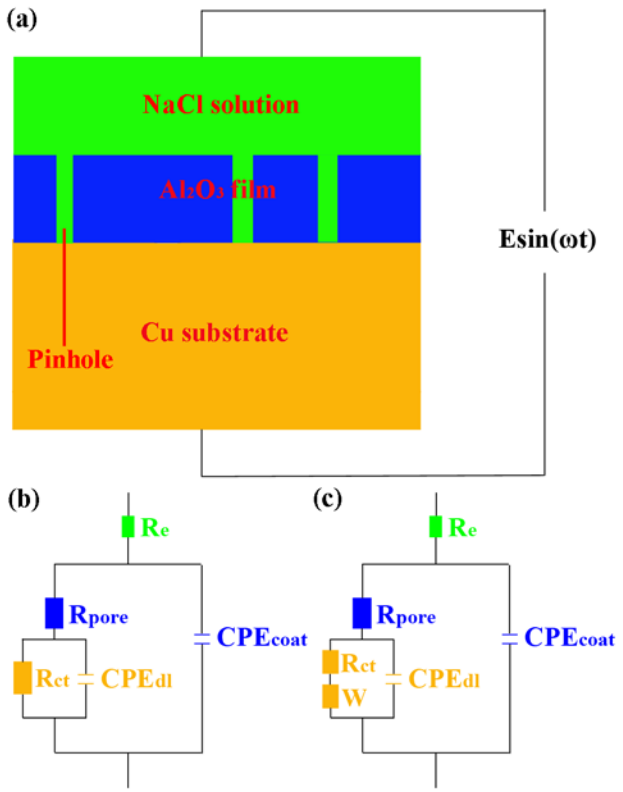

Figure 4. (a) Diagram of the test system. Al_2O_3 film coated copper is immersed in a 0.1 M NaCl aqueous solution, and a disturbance sinusoidal voltage $E\sin(\omega t)$ is applied to the system. (b) ECs used to describe the Al_2O_3 film coated copper substrate. (c) ECs used to describe the bare copper substrate.

Figure 5 shows the EIS data for the copper substrate and Al_2O_3 film coated samples presented as Bode plots (impedance module and phase angle vs. log(freq)). Two time constants can be observed in the spectra, which is consistent with the model proposed. The phase angle in the high frequency region gives information on film capacitance. With the increase of film thickness, film capacitance decreases, and phase angle in the high frequency region increases, indicating enhanced capacitive behavior. The impedance in the low frequency region corresponds to the film resistance. The increase of impedance is observed with the increase of film thickness, indicating increasing corrosion resistance.

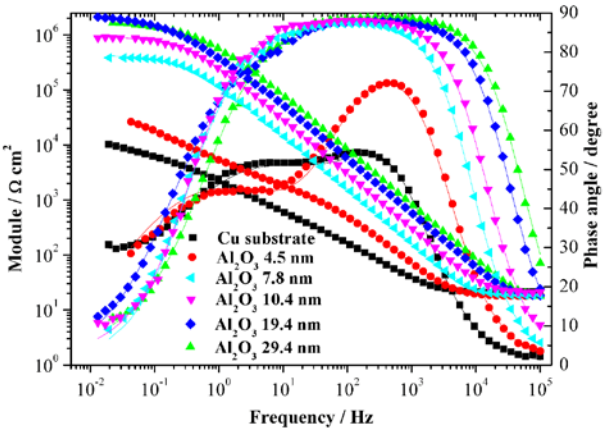

Figure 5. The EIS data for the copper substrate and Al_2O_3 film coated samples.

Because the Al_2O_3 film possesses high electric insulativity, anodic oxidation rarely occurs on the surface of the film. Instead, in the pinholes of the film, where electrolyte contacts with the copper substrate directly, that anodic reaction mostly occurs. The EIS fitting parameters obtained using the equivalent circuit presented in Figure 4 (b) and (c) are listed in Table 1. The polarization resistance R_p can be obtained from pore resistance R_{pore} and charge transfer resistance R_{ct} present in Table 1,[23]

$$R_p = R_{pore} + R_{ct} \qquad (3)$$

and then porosity (pinhole induced uncoated substrate surface fraction) of the Al_2O_3 films can be determined from the equation in our previous study.[19] Figure 6 shows the porosity of the Al_2O_3 film coated samples. The porosity decreases with the increase of film thickness. This is why the corrosion resistance increases with the increasing film thickness. The porosity of Al_2O_3 film tends to become stable as film thickness increases to 7.8 nm. When the film thickness further increases, the porosity decreases slowly. This means that a 7.8 nm thick Al_2O_3 film is effective in reducing copper corrosion.

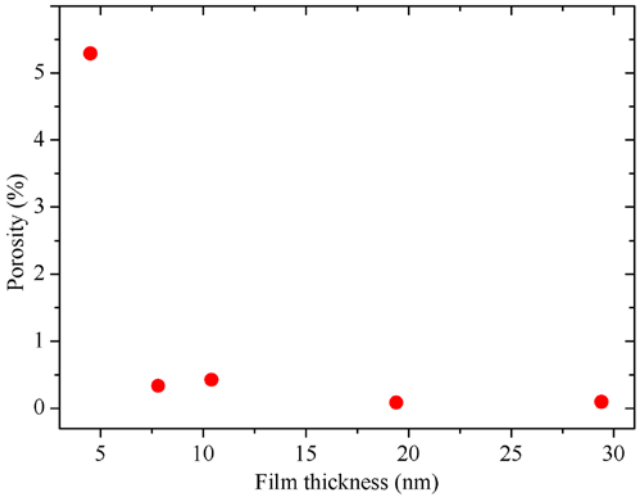

Figure 6. The porosities of the Al_2O_3 films.

Figure 7 (a) shows the SEM image of the copper substrate before corrosion. The surface is smooth with no defect, which consists with the result obtained by AFM. Figure 7 (b) shows the SEM image of the copper substrate after corrosion. The copper substrate is corroded and many fine structures developed on its surface. These fine structures are grain boundaries of polycrystalline copper.[34-36, 29] Figure 7 (c) is a magnified image of the selected area in (b) from which the grain boundaries can be clearly seen. When the copper substrate is coated with a 4.5 nm Al_2O_3 film, the corrosion of copper substrate decreases greatly, as shown in Figure 7 (d). However, a 4.5 nm Al_2O_3 film is still insufficient to protect copper from corrosion as the porosity is still high, 5.29%. A mass of pinholes can be observed on the surface of the film. Figure 7 (e) shows a magnified image of the pinholes in the selected area of (d). After a 7.8 nm Al_2O_3 film is deposited, the porosity decreases to 0.33% and the surface of copper substrate is well protected. It can be seen from Figure 7 (f) that no obvious corrosion is observed.

Table 1. The EIS fitting parameters obtained using the equivalent circuits presented in Figure 4 (b) and (c).

Samples	R_e (Ω cm^2)	CPE_{coat} ($\mu\Omega^{-1}$ cm^{-2} s^n)	n_{coat}	R_{pore} (kΩ cm^2)	CPE_{dl} ($\mu\Omega^{-1}$ cm^{-2} s^n)	n_{dl}	R_{ct} (kΩ cm^2)	W ($\mu\Omega^{-1}$ cm^{-2} $\sqrt{s}$)
Cu	20.6	15.40	0.887	0.23	112	0.610	9.09	465
4.5 nm Al_2O_3	17.7	3.92	0.944	1.22	58.5	0.600	46.7	-
7.8 nm Al_2O_3	23.9	0.86	0.991	12.4	0.55	0.568	675	-
10.4 nm Al_2O_3	18.9	0.51	1	38.0	0.41	0.504	852	-
19.4 nm Al_2O_3	16.7	0.27	1	76.6	0.36	0.569	2360	-
29.4 nm Al_2O_3	15.2	0.19	1	292	0.42	0.423	1800	-

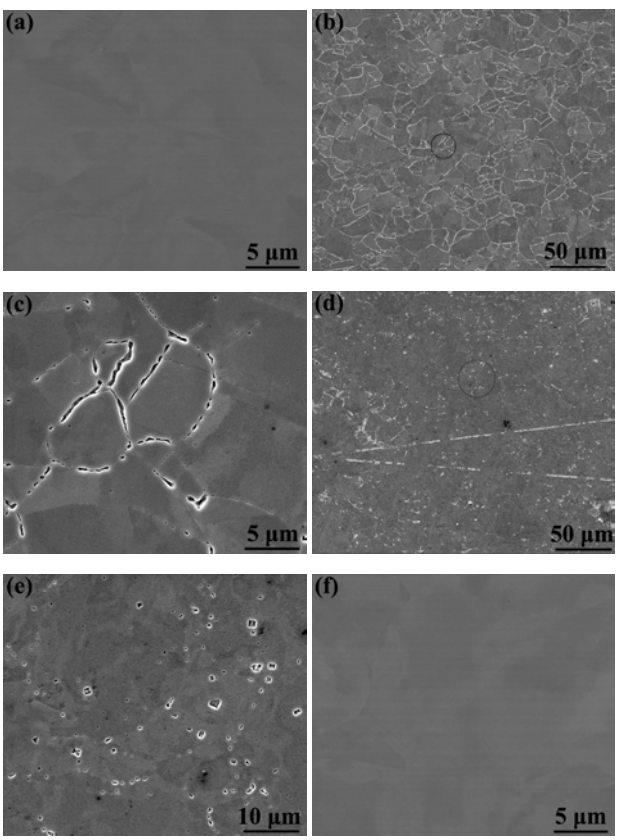

Figure 7. (a) SEM image of the polished copper substrate before EIS measurement. (b) SEM image of the copper substrate after EIS measurement. (c) A magnified image of the selected area in (b). (d) SEM image of the 4.5 nm Al_2O_3 film coated copper substrate after EIS measurement. (e) A magnified image of the selected area in (d). (f) SEM image of the 7.8 nm Al_2O_3 film coated copper substrate after EIS measurement.

Figure 8 (a) shows the AFM image of the copper substrate after corrosion. The surface of the copper substrate becomes rough after corrosion and the depth of the grain boundary increases. The surface of the 4.5 nm Al_2O_3 film coated copper substrate (Figure 8 (b)) is also rough because the porosity is still high, while the surface of the 7.8 nm Al_2O_3 film coated copper substrate (Figure 8 (c)) is nearly identical to that of the initial copper substrate because of the low film porosity. The RMS roughness values of corroded surface in Figure 8 (d) decrease with the increasing film thickness, which is in good agreement with the film porosity.

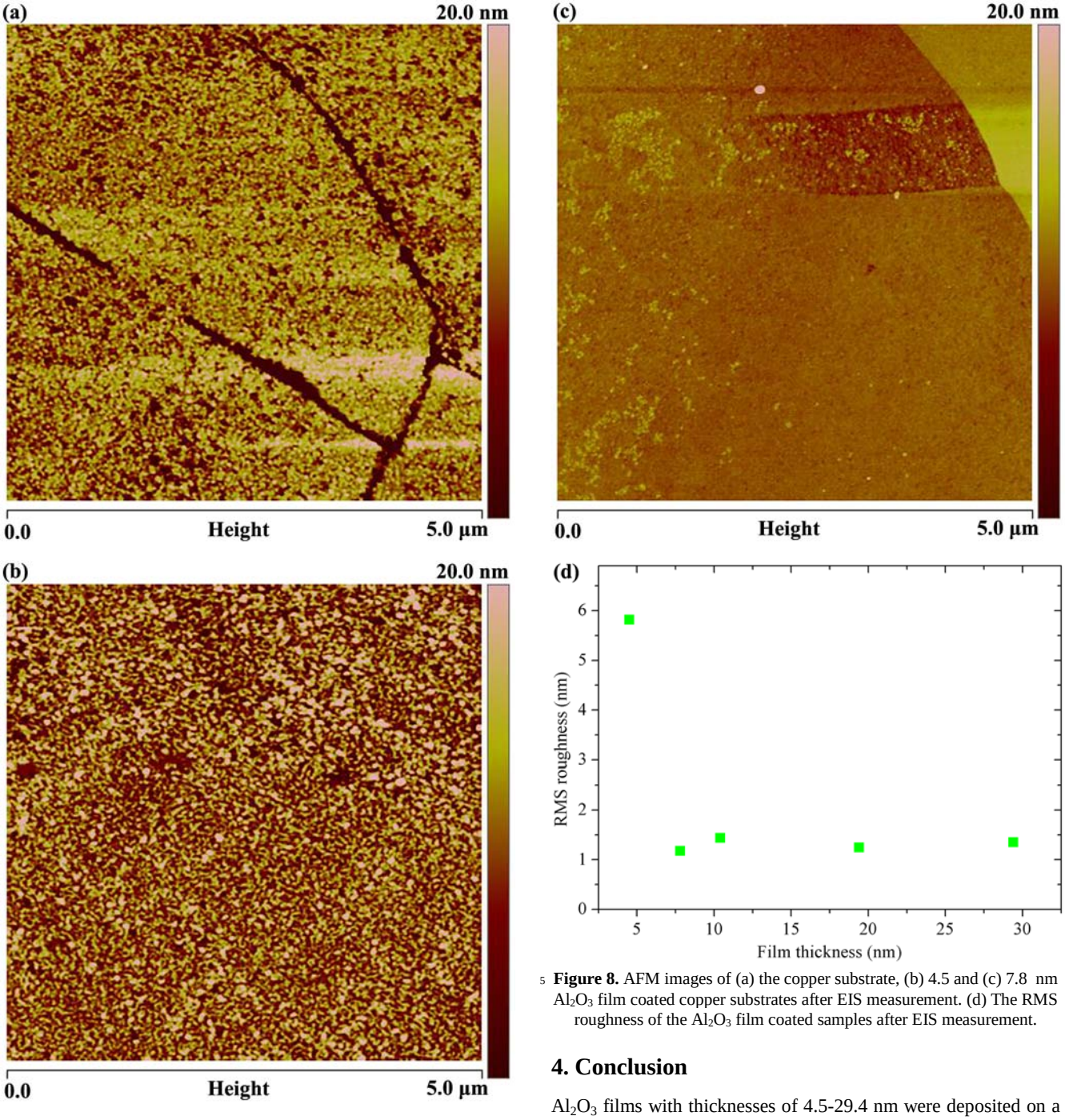

Figure 8. AFM images of (a) the copper substrate, (b) 4.5 and (c) 7.8 nm Al_2O_3 film coated copper substrates after EIS measurement. (d) The RMS roughness of the Al_2O_3 film coated samples after EIS measurement.

4. Conclusion

Al_2O_3 films with thicknesses of 4.5-29.4 nm were deposited on a fine polished copper substrate by ALD. Due to the self-limiting growth mechanism of the ALD process, Al_2O_3 films were coated conformally on the copper substrate. The morphology of the uncoated does not differ greatly from that of the coated copper substrate. Surface and depth profile element analysis show that the Al_2O_3 films are well stoichiometric. EIS measurement demonstrates that the Al_2O_3 films can significantly improve the corrosion resistance of copper in a 0.1 M NaCl solution. With the increase of film thickness, the corrosion resistance of the Al_2O_3 films increases. High corrosion resistance of thick Al_2O_3 films is attributed to their low porosity. The porosity of Al_2O_3 films becomes stable as film thickness increases to 7.8 nm. With the further increase of film thickness, the porosity decreases slowly.

Therefore, a 7.8 nm Al_2O_3 film is capable of protecting copper from corrosion. From AFM and SEM images, it can be seen that the 7.8 nm coated copper surface is not corroded.

Acknowledgements

The authors greatly appreciate the financial support of the National Science Fund for Distinguished Young Scholars (50825501), the Science Fund for Creative Research Groups (51321092), the National Natural Science Foundation of China (51335005 and 91323302), and the National Science and Technology Major Project (2008ZX02104-001). Helpful discussions with Wen Jing are gratefully acknowledged.

Notes and references

[a] *The State Key Laboratory of Tribology, Tsinghua University, Beijing 100084, China. Telephone/Fax: +86 10 6279 7362; E-mail addresses: xclu@tsinghua.edu.cn*
[b] *College of Mechanical and Electrical Engineering, China University of Petroleum, Qingdao 266580, China*
[c] *National Engineering Research Center for Nanotechnology, Shanghai 200241, China*

1 S. H. Lee, J. G. Kim and J. Y. Koo, *Eng. Failure Anal.*, 2010, **17**, 1424.
2 L. Bin, W. J. Meng and M. Fanghua, *J. Micromech. Microeng.*, 2013, **23**, 35017.
3 M. Rabbani, I. Dincer, G. E. Naterer and M. Aydin, *Int. J. Hydrogen Energy*, 2012, **37**, 11021.
4 A. Armanious and K. Johannsen, *Mater. Corros.*, 2012, **63**, 438.
5 E. Sarver and M. Edwards, *Mater. Perform.*, 2011, **50**, 60.
6 B. Jeon, S. Sankaranarayanan, A. van Duin and S. Ramanathan, *J. Chem. Phys.*, 2011, **134**, 234706.
7 O. E. Farooqi, G. V. Loganathan, M. A. Edwards, D. Bosch, J. Lee and P. Scardina, *J. Water Resour. Plann. Manage.*, 2009, **135**, 227.
8 B. Li, H. Zhou, H. Song, Q. Xiao and X. Li, *Ind. Water Treat.*, 2006, **26**, 4.
9 M. D. Groner, J. W. Elam, F. H. Fabreguette and S. M. George, *Thin Solid Films*, 2002, **413**, 186.
10 M. Leskela and M. Ritala, *Thin Solid Films*, 2002, **409**, 138.
11 M. Leskela and M. Ritala, *Angew. Chem. Int. Ed.*, 2003, **42**, 5548.
12 B. Diaz, J. Swiatowska, V. Maurice, A. Seyeux, B. Normand, E. Harkonen, M. Ritala and P. Marcus, *Electrochim. Acta*, 2011, **56**, 10516.
13 B. Diaz, E. Harkonen, J. Swiatowska, V. Maurice, A. Seyeux, P. Marcus and M. Ritala, *Corros. Sci.*, 2011, **53**, 2168.
14 B. Diaz, E. Harkonen, V. Maurice, J. Swiatowska, A. Seyeux, M. Ritala and P. Marcus, *Electrochim. Acta*, 2011, **56**, 9609.
15 S. E. Potts, L. Schmalz, M. Fenker, B. Diaz, J. Swiatowska, V. Maurice, A. Seyeux, P. Marcus, G. Radnoczi, L. Toth and W. Kessels, *J. Electrochem. Soc.*, 2011, **158**, C132.
16 E. Harkonen, S. E. Potts, W. Kessels, B. Diaz, A. Seyeux, J. Swiatowska, V. Maurice, P. Marcus, G. Radnoczi, L. Toth, M. Kariniemi, J. Niinisto and M. Ritala, *Thin Solid Films*, 2013, **534**, 384.
17 A. I. Abdulagatov, Y. Yan, J. R. Cooper, Y. Zhang, Z. M. Gibbs, A. S. Cavanagh, R. G. Yang, Y. C. Lee and S. M. George, *ACS Appl. Mater. Interfaces*, 2011, **3**, 4593.
18 Y. D. Zhang, D. Seghete, A. Abdulagatov, Z. Gibbs, A. Cavanagh, R. G. Yang, S. George and Y. C. Lee, *Surf. Coat. Technol.*, 2011, **205**, 3334.
19 Z. Chai, J. Li, X. Lu and D. He, *RSC Advances*, 2014, DOI: 10.1039/C4RA04565C.
20 R. Matero, A. Rahtu, M. Ritala, M. Leskela and T. Sajavaara, *Thin Solid Films*, 2000, **368**, 1.
21 Z. Chai, Y. Liu, X. Lu and D. He, *Tribol. Lett.*, 2014, **55**, 143.
22 W. Tato and D. Landolt, *J. Electrochem. Soc.*, 1998, **145**, 4173.
23 C. Liu, Q. Bi, A. Leyland and A. Matthews, *Corros. Sci.*, 2003, **45**, 1257.
24 C. Liu, Q. Bi, A. Leyland and A. Matthews, *Corros. Sci.*, 2003, **45**, 1243.
25 G. J. Brug, A. Vandeneeden, M. Sluytersrehbach and J. H. Sluyters, *J. Electroanal. Chem.*, 1984, **176**, 275.
26 M. Valcarce, S. R. De Sanchez and M. Vazquez, *J. Mater. Sci.*, 2006, **41**, 1999.
27 F. Brizuela, R. Procaccini, S. Cere and M. Vazquez, *J. Appl. Electrochem.*, 2006, **36**, 583.
28 B. Trachli, M. Keddam, H. Takenouti and A. Srhiri, *Corros. Sci.*, 2002, **44**, 997.
29 Y. Van Ingelgem, A. Hubin and J. Vereecken, *Electrochim. Acta*, 2007, **52**, 7642.
30 G. P. Cicileo, B. M. Rosales, F. E. Varela and J. R. Vilche, *Corros. Sci.*, 1999, **41**, 1359.
31 E. M. Sherif and S. M. Park, *Electrochim. Acta*, 2006, **51**, 4665.
32 W. A. Badawy, K. M. Ismail and A. M. Fathi, *Electrochim. Acta*, 2005, **50**, 3603.
33 X. N. Liao, F. H. Cao, L. Y. Zheng, W. J. Liu, A. N. Chen, J. Q. Zhang and C. A. Cao, *Corros. Sci.*, 2011, **53**, 3289.
34 L. Lapeire, E. M. Lombardia, K. Verbeken, I. De Graeve, L. Kestens and H. Terryn, *Corros. Sci.*, 2013, **67**, 179.
35 J. K. Yu, E. H. Han, L. Lu, X. J. Wei and M. Leung, *J. Mater. Sci.*, 2005, **40**, 1019.
36 Y. Van Ingelgem, E. Tourwe, J. Vereecken and A. Hubin, *Electrochim. Acta*, 2008, **53**, 7523.